

# Multicomponent scalar dark matter at high-intensity proton beam experiments

Amalia Betancur,<sup>1,\*</sup> Andrés Castillo,<sup>2,3,4,†</sup> Guillermo Palacio,<sup>1,‡</sup> and Juan Suarez<sup>1,§</sup>

<sup>1</sup>*Grupo Física Teórica y Aplicada, Universidad EIA,  
A.A. 7516, Envigado, Colombia*

<sup>2</sup>*Grupo de Física Experimental, Big Data y Analítica, Universidad Sergio Arboleda,  
Bogotá DC, Colombia*

<sup>3</sup>*Instituto de Astrofísica de Canarias, C/ Vía Láctea, s/n E38205  
La Laguna (Tenerife), Spain*

<sup>4</sup>*Universidad de La Laguna, Departamento de Astrofísica, La Laguna, Tenerife, Spain  
La Laguna (Tenerife), Spain*

We study a scalar dark matter (DM) model with two DM species coupled to the Standard Model (SM) particles via a sub-GeV dark photon. In this model, we find that DM conversion occurs through the dark photon and it plays a fundamental role in setting the observed relic abundance. Furthermore, the two DM candidates can be produced at fixed-target experiments a la Beam-Dump. Detailed predictions for signal and backgrounds are obtained with the help of MadDump and NuWro Montecarlo generators. We explore the potential reach on the sensitivity of DUNE near detector and SHiP experiment, and we find that portions of the parameter space will be within reach of the two experiments.

## I. INTRODUCTION

Despite the increasing evidence of the existence of dark matter (DM), its direct observation continues to be elusive. Many searches for DM have been carried out in a variety of experiments, in indirect detection looking for signals of DM annihilation in outer space, underground facilities looking for DM interaction with a detector, and even at the Large Hadron Collider, all yielding null results so far. The DM program has mostly focused on the search for a DM particle at the electroweak scale, because it has been considered that such mass scale is natural for a Weakly Interactive Massive Particle (WIMP), one of the preferred DM candidates. Nevertheless, the null results so far, have prompted the community to consider different candidates and/or mass ranges. For instance, DM candidate could still be a WIMP with thermal decoupling but with a mass that lies well below the electroweak scale and is therefore not within reach of the usual direct detection experiments sensitive to weak scale WIMPS. It is then natural that such DM candidate has escaped observation.

For this DM to communicate with the SM a new portal is needed, which could be scalar, vector or fermion [1]. One of the most widely studied models is the vector portal, where the mediator is a new gauge boson, similar to the photon, which communicates to the SM through a kinetic mixing [2–14]. Such new gauge boson, the dark photon, has previously been proposed to explain the observation of gamma-ray lines in the center of the Milky Way [2] and the discrepancy between the theoretical prediction and the measured value of the muon anomalous magnetic moment  $\Delta a_\mu$  [15, 16], as is included in the historical account of [17]. In this work we will consider a dark photon that arises from a  $U(1)_D$  symmetry, which is broken, hence yielding a massive vector boson. This dark photon will not be considered for the aforementioned reported anomalies, but as a portal to communicate the DM sector with the SM sector.

In regards to the DM particles that communicate with the SM through the dark photon, the preferred candidates have been singlets, either fermion or scalar particles that are only charged under the  $U(1)_D$  symmetry. Nevertheless, it is important to consider models that go beyond the simplest scenarios and that have more potential for rich phenomenology. For instance, the total relic abundance could be saturated by several DM candidates, which is natural considering that 5% of the matter-energy content of the Universe is made of a myriad of particles. This idea, dubbed multicomponent DM has gained more attention because it introduces viable candidates while also allowing for a rich phenomenology that could be within reach of actual and near-future experiments. Such models allow

\* amalia.betancur@eia.edu.co

† acastillo@iac.es

‡ guillermo.palacio38@eia.edu.co

§ juan.suarez47@eia.edu.co

for different parameter space than the one-component and may include important effects such as DM conversion. Moreover, we know DM is multicomponent because active neutrinos make up a small percentage of the DM [18]. Thus, it makes sense to consider more than one DM particle.

Facilities that rely on high-intensity proton collisions have a great potential to look for dark-sector models, because in the energetic collisions it is possible to produce the dark sector particles which could be detected through interactions such as electron recoil. Those interactions have the potential to probe low masses, and although there could be a large background coming from neutrinos, it is also possible to disentangle the two types of events. This is the case of DUNE (Deep Underground Neutrino Experiment) [19] and SHiP (Search for Hidden Particles) [20] experiments.

For instance, DUNE-LBNF (Long-Baseline Neutrino Facility) will use a high-intensity proton beam of 120 GeV producing a flux of neutrinos with energies in the range of several hundreds of MeVs up to several GeVs. DUNE will also have two state-of-the-art near and far detectors, composed mainly of liquid argon. For the near detector (ND), the Precision Reaction of Independent Spectrum Measurement (PRISM) concept incorporates a moving complex across different off-axis positions [21]. The PRISM idea allows to control systematically the uncertainties from neutrino flux measurements and neutrino-nucleus interactions (i.e. cross sections constraints); and thus improve the precision tests for neutrino oscillations [22]. Besides, as we will show in this paper, the PRISM concept leads to a background reduction, converting the DUNE ND into a crucial experiment to search for dark-sector particles produced after the collision of the proton beam with the target.

In this work, we consider a DM model where two singlet scalars are the DM candidates, both charged under the  $U(1)_D$  symmetry and under discrete symmetries that ensure the stability of both DM candidates. The relic density phenomenology is presented, including the impact of DM conversion. In addition, we investigate the potential reach on the sensitivity of the two-component scalar dark matter model. For that aim, we consider two currently under construction experiments: DUNE and SHiP. In particular, we consider a dark photon in the mass window of 10 – 900 MeV with on-shell decay to scalar DM and study the expected sensitivity of the experiment on the parameter space of the model. For the construction of the sensitivity, we compare the neutrino-electron ( $\nu-e$ ) scattering (the background) against the DM-electron (DM- $e$ ) scattering (the signal). Our results are novel and go beyond the analyses presented in Refs. [23–26] in the following ways:

- We propose a model with two dark matter components, leading to new annihilation channels, impacting the relic density. Additionally, we perform a comprehensive exploration of the parameter space of the model given by the relic abundance observable.
- Regarding the background studies, we show that the NuWro Monte Carlo generator is suitable to simulate neutrino-induced events in the DUNE-ND.
- Moreover, we show that the SHiP experiment is crucial in obtaining the most stringent constraints of the sensitivity for the multicomponent model.
- For two dark matter component, DUNE-ND and SHiP experiments allow us to explore different parameter space compared to the one allowed for the one dark matter candidate model.

This paper is organized as follows: In Sec. II we introduce the model Lagrangian, particle content and list the tools used in the phenomenological study for this work. In Sec. III we present the constraints on DM observables, discuss DM conversion, and investigate the phenomenological implications of two dark matter candidates. Sec. IV discusses the experimental set-up for light DM production at high-intensity proton beam experiments, and displays some relevant results regarding the background and signal simulation. Additionally, we show the advantages of moving the DUNE ND to off-axis configurations. We also present the potential reach on the sensitivity for DUNE and SHiP in Sec. V. Finally, our results are summarized in Sec. VI.

## II. THE MODEL

We consider an extension of the SM by adding two new gauge singlets to the scalar sector. One complex singlet is charged under a new global symmetry  $Z_2$  and the other one is charged under a  $Z'_2$ , while the SM particles are uncharged. These symmetries will remain unbroken rendering two stable DM candidates that may coexist. There is also a new  $U(1)_D$  symmetry with only the added scalar sector being charged under it. This symmetry is broken, so that there is a new massive gauge boson. The gauge Lagrangian associated to the two  $U(1)$  symmetries [2, 3], the SM and dark symmetry is:

$$\mathcal{L}_{\text{gauge}} = -\frac{1}{4}F_{\mu\nu}F^{\mu\nu} - \frac{1}{4}F'_{\mu\nu}F'^{\mu\nu} - \frac{\varepsilon}{2}F_{\mu\nu}F'^{\mu\nu} , \quad (1)$$

where,  $F_{\mu\nu}$  and  $F'_{\mu\nu}$  are the field strength tensors associated to the  $U(1)_Y$  and  $U(1)_D$  symmetries. The last term of Eq. (1) implies that there is a mixing between the gauge bosons associated to the two symmetries which after diagonalization results in a massless gauge boson, the photon  $\gamma$ , and a massive one, the dark photon  $\gamma'$  [2, 3]. The dark photon acquires its mass once a new complex singlet scalar field develops a vacuum expectation value (v.e.v). A similar scenario was studied in Ref. [5, 27, 28]. The presence of this new scalar field does not affect the phenomenology of the model due to the choice of its v.e.v and the chosen parameters presented in III C, and thus we do not discuss it any further. On the other hand, it has been shown that it is possible for this kinetic mixing to vanish [29], nevertheless, this term will not vanish when a transformation of the gauge fields involves an off-diagonal element, as is considered in this work and previous works such as [14]. Moreover, it has been proposed that the phenomenology associated with this kinetic mixing could be explored at neutrino experiments [30, 31], or high- intensity proton beam experiments.

The scalar potential of the added sector which sets the interaction of the new complex singlets  $\phi_1$ ,  $\phi_2$  and the SM Higgs doublet,  $H$  reads:

$$V(H, \phi_1, \phi_2) = \mu_{\phi_1}^2 |\phi_1|^2 + \mu_{\phi_2}^2 |\phi_2|^2 + \lambda_{\phi_1} |\phi_1|^4 + \lambda_{\phi_2} |\phi_2|^4 + \lambda_{\phi_1 H} |\phi_1|^2 (H^\dagger H) + \lambda_{\phi_2 H} |\phi_2|^2 (H^\dagger H) + \lambda_{\phi_1 \phi_2} |\phi_1|^2 |\phi_2|^2, \quad (2)$$

with the last term of the potential implying that the two added scalars may interact with each other. It is important to note that in this potential, both the complex and imaginary part of each  $\phi_i$  field have the same mass. This is due to the imposed symmetries. As a result, the DM candidates are the  $\phi_i$  fields. Similar scenarios have been studied in Ref. [32, 33]. On the other hand, each new scalar field may interact with SM particles as well as the other scalar field via the dark photon portal. As a result, this portal will be fundamental in setting the phenomenology of the model. Subsequently the new parameters that will have an important effect in the DM phenomenology are the dark fine structure constant  $\alpha_D$ , the kinetic mixing  $\varepsilon$ , and the new particles  $\phi_1$ ,  $\phi_2$ , and  $\gamma'$ .

In order to explore the phenomenology, the model was implemented in SARAH [34] based on the model developed in Ref. [35]. The SARAH package allows for calculations of the relevant interactions among particles, performs anomaly checks and generates output to other packages such as SPHENO [36, 37], which calculates the mass spectrum and other relevant parameters. SARAH also provides a link to other packages like MicrOMEGAS [38] which calculates DM observables (relic abundance, spin independent (SI), and spin dependent (SD) cross sections), MadGraph [39] including its plugin MadDump [40] which allows for a simulation of DM interaction with electrons at DUNE and SHIP. For the case of DUNE, we include on-axis and DUNE-PRISM analyses. On the other hand, to simulate the production of DM particles at proton collisions we used PYTHIA [41, 42]. Furthermore, neutrino-electron interactions are similar to those of DM particles, so they must be included in the analysis as background; for such processes we used the Monte Carlo generator NuWro [43, 44].

### III. DARK MATTER PHENOMENOLOGY

Since this model presents two stable DM candidates that interact with the dark photon, it has a rich phenomenology that could be explored or constrained through the measured relic density as well as direct detection (DD) experiments that are sensitive to low DM masses.

#### A. Dark matter constraints

Before exploring the allowed parameter space of the model and choosing appropriate benchmark points, one must consider the different restrictions arising from DM observables:

- Following the Planck satellite measurement [45], we consider models that fulfill the relic abundance as those that satisfy:

$$\Omega h^2 = 0.1200 \pm 0.0012, \quad (3)$$

allowing a  $3\sigma$  departure from the central value.

- The DM self interaction cross section is constrained, by observations of galaxy cluster collisions, to be

$$\frac{\sigma}{m_{DM}} \lesssim \text{few} \times \text{cm}^2/\text{g}, \quad (4)$$

this imposes limits on the allowed value of  $\alpha_D$ . For the DM masses considered in this work,  $\alpha_D \lesssim 0.5$  [26].

## B. Dark matter relic density general framework

Because each of these DM candidates,  $\phi_1$  and  $\phi_2$ , is a singlet under the SM symmetries, in principle, few or no channels are available for DM annihilation in the early Universe, thus tending to yield an overabundant density. Nevertheless, due to the presence of the new  $U(1)_D$  symmetry and the kinetic mixing between  $\gamma$  and  $\gamma'$ , new annihilation channels appear which allows the DM relic density to be at the observed values for certain portions of the parameter space. In principle, the thermally averaged annihilation cross section is set by the process  $\phi\phi \rightarrow \gamma' \rightarrow f\bar{f}$ , which depends on dark sector parameters such as  $m_{\phi_i}$ ,  $m_{\gamma'}$ ,  $\varepsilon$ , and  $\alpha_D$ , as stated in Ref. [46]. Here  $f$  denotes a SM fermion, while  $\bar{f}$  denotes a SM anti fermion. This annihilation channel is available as long as the mass of the DM is larger than the electron mass which is the case studied here. This scenario has been investigated in many works such as [23, 47, 48]. Nevertheless, for the present model, the relic abundance could depart from that of previous models due to additional annihilation channels, mainly  $\phi_i^* \phi_i \rightarrow \phi_j^* \phi_j$  where  $i, j$  denote either the  $Z_2$  and  $Z'_2$  charged scalar particle (shown in the left panel of Fig. 1) and through  $\phi_i \phi_i^* \phi_j \phi_j^*$  which is set by the four contact interaction controlled by the coupling  $\lambda_{\phi_1 \phi_2}$ , (shown in right panel of Fig. 1). These are known as the DM conversion channels, and it has been shown that they may have a profound effect on the relic density [49].

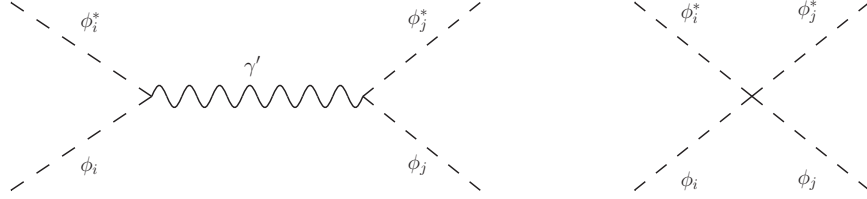


FIG. 1. Possible DM conversion channels of the model: Left panel, mediated by the dark photon. Right panel, the four contact interaction.

## C. Relic density and dark matter conversion

In order to study DM relic abundance, we used **MicrOMEGAS-5.2.4** [38] which allows two DM candidates, giving valuable information about the different annihilation channels that are relevant for a certain point of the parameter space.

Because the parameter space is large, we focus on the scenario where  $m_{\gamma'} = 3 m_{\phi_1}$  and  $\alpha_D = 0.1$ , a scenario widely studied in works such as [23, 25, 47]. This benchmark point allows for a free choice of  $m_{\phi_2}$ . Next, we focus on two scenarios for  $m_{\phi_2}$ , one where it is fixed and one where  $m_{\phi_2} - m_{\phi_1} = \text{constant}$ . We also set the scalar potential couplings as follows:

$$\lambda_{\phi_1 H} = \lambda_{\phi_2 H} = 10^{-10}, \quad \lambda_{\phi_1} = \lambda_{\phi_2} = 0.1, \quad \lambda_{\phi_1 \phi_2} = (0 - 3.0). \quad (5)$$

Additionally, the coupling of the scalar singlet – responsible of the  $U(1)_D$  symmetry breaking– to the  $\phi_i$  scalar fields is of the same order than  $\lambda_{\phi_i H}$ . For the case of fixed mass of the heavy DM particle, we set  $m_{\phi_2} = 1.0$  and  $0.1$  GeV. The results of the relic abundance of the light DM particle for this scan are shown in the left panel of Fig. 2. As can be seen, for the case of  $m_{\phi_2} = 0.1$  GeV, once  $\phi_1$  becomes heavier than  $\phi_2$ , its relic abundance becomes suppressed, indicating that this DM particle is being depleted. To further understand this behavior, we present the relic abundance of each DM particle for  $m_{\phi_2} = 0.1$  GeV on the right panel. As is shown,  $\Omega h_{\phi_2}^2$  is constant, underabundant, and several orders of magnitude smaller than  $\Omega h_{\phi_1}^2$  until  $m_{\phi_1} > m_{\phi_2}$ . At this point the  $\phi_2$  abundance tracks the previous behavior of  $\phi_1$  while  $\phi_1$  is depleted. This is showing two important things: one, the DM conversion channel is very efficient and proceeds as long as it is viable, two, once the hierarchy of the DM particles mass is inverted, the two particles switch roles. This last point is expected since the two particles have the same behavior under the symmetry groups, thus, the parameter that dominates which DM remains and which gets depleted is the mass ordering. This last point also implies that for  $m_{\phi_2} - m_{\phi_1} = \text{constant}$  we obtain the same results as the case where  $m_{\phi_2} = 1.0$  GeV (same mass ordering). Thus we will not comment any more on this scenario.

Another interesting trend shown both in the left and right panel is that for  $m_{\phi_1} \lesssim 0.02$  GeV the relic abundance declines with the DM mass value, yet for  $m_{\phi_1} > 0.02$  GeV this behavior changes. To explore this, we used the **MicrOMEGAS-5.2.4** function that allows for exclusion of certain annihilation channels, such as DM conversion. For

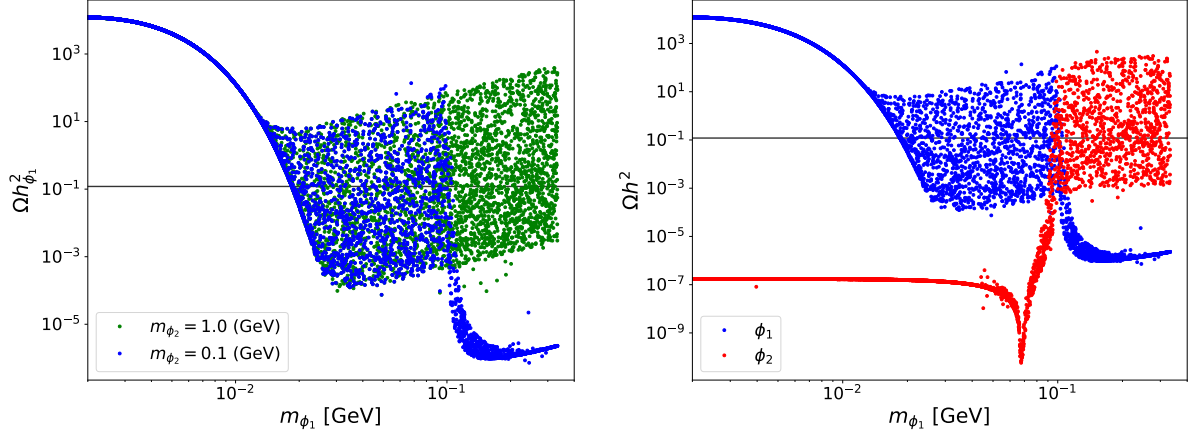


FIG. 2. The left panel shows the relic abundance of  $\phi_1$  vs. its mass, with  $m_{\phi_2} = 1.0(0.1)$  GeV for the green (blue) dots. The right panel shows the relic abundance of  $\phi_1$  ( $\phi_2$ ) in blue (red) vs  $m_{\phi_1}$  for  $\phi_2 = 0.1$  GeV. For both plots, we set  $m_{\gamma'} = 3 m_{\phi_1}$ , while the grey horizontal band corresponds to the measured value of the DM relic abundance.

this, we computed the relic abundance allowing all channels and without the DM conversion channel. The results are presented in Fig. 3 where we set  $\varepsilon^2 = 10^{-6}$  and  $m_{\phi_2} = 0.1$  GeV. The difference between all allowed channels (green) and channels without DM conversion (magenta) shows is that for  $m_{\phi_1} \lesssim 0.02$  GeV, DM conversion channels are not efficient, which means that the relic abundance is set by the annihilation of two  $\phi_1$  into SM particles. However, once  $m_{\phi_1} \gtrsim 0.02$  GeV the DM conversion channel becomes available and starts to dominate, leading to a significant suppression of the relic abundance compared to the case where there is no conversion. Again, this exhibits the importance of DM conversion on the relic density of the model. It is important to add that this channel proceeds only via the exchange of a dark photon (left panel of Fig. 1), that is because the other possibility, which is the four contact interaction (right panel of Fig. 1), shows no effect on the relic density when varying  $\lambda_{\phi_1\phi_2}$ .

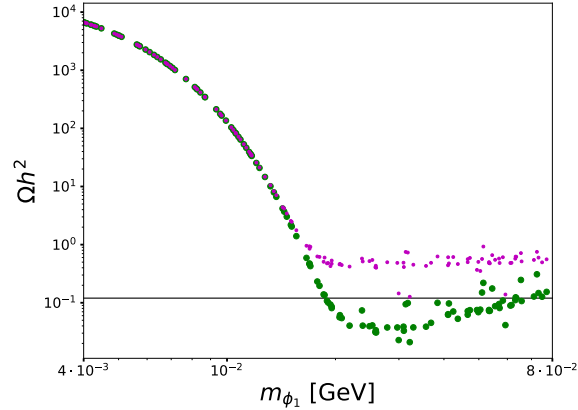


FIG. 3. Relic abundance vs.  $m_{\phi_1}$  for all channels (green) and all channels except the DM conversion channels (magenta) with  $\varepsilon^2 = 10^{-6}$ ,  $m_{\gamma'} = 3 m_{\phi_1}$  and  $m_{\phi_2} = 0.1$  GeV.

#### D. DM direct detection

An interesting way to probe DM models is by looking for the evidence of the recoil of a DM particle with a detector located on Earth, this is known as DM direct detection (DD). Due to the interactions of the DM with the dark photon, it is possible for it to recoil against a nucleon via a spin independent (SI) interaction. The CRESST-III experiment [50] has the potential to probe a portion of the DM masses considered here, thus we study if the parameter space is

constrained by the experiment. To do so, we again use `MicrOMEGAS-5.2.4` [38] which allows for the calculation of the DM-nucleon SI cross section. Nevertheless, we can not directly use the experiment's constraints on the SI cross section due to the following considerations that must be taken into account here:

1. Due to the presence of two DM candidates, we must rescale CRESST-III restrictions because DD experiments place constraints assuming that one DM particle saturates the relic abundance which has implications on its density in the Earth and then on the expected event rate. For two DM particles the density in the Earth is smaller than for one candidate, thus, we must rescale the cross section in order to impose the restrictions. This is done as follows [51]:

$$\frac{\delta_{\phi_1^0}}{m_{\phi_1^0}}\sigma_{\phi_1^0} + \frac{\delta_{\phi_2^0}}{m_{\phi_2^0}}\sigma_{\phi_2^0} < \frac{\sigma_0}{m_0} , \quad (6)$$

where  $\delta_{\phi_1^0}(\delta_{\phi_2^0})$  is the fraction of the  $\phi_1^0(\phi_2^0)$ ,  $\sigma_{\phi_1^0}(\sigma_{\phi_2^0})$  is the scattering cross section of the  $\phi_1^0(\phi_2^0)$  particle with a nucleon. The parameters associated to the experiment's sensitivity are  $\sigma_0$  and  $m_0$  which are related to the measured experimental event rate  $R_{exp} \sim \rho_0 \sigma_0 m_0$ .

2. DD experiments also impose restriction on the DM-nucleon scattering cross section assuming that DM couples equally to protons and neutrons. Nevertheless, this is not always the case, a DM model could show isospin violation. For the present model, we find that DM particles exhibit such violation. This, again, implies that the cross-section must be rescaled, and works such as [52, 53] have found that such procedure must be done as follows:

$$\frac{\sigma_p}{\sigma_N^Z} = \frac{\sum_i \eta_i \mu_{A_i}^2 A_i^2}{\sum_i \eta_i \mu_{A_i}^2 [Z + (A_i^2 - Z)f_n/f_p]^2} . \quad (7)$$

Here,  $\sigma_p$  and  $\sigma_N^Z$  are the DM-nucleus and DM-nucleon SI cross section, respectively. This equation takes into account that the DM detector could be composed of different isotopes  $A_i$  with  $\eta_i$  being the fractional abundance of the isotope,  $\mu_{A_i}$  is the DM-nucleus reduced mass,  $Z$  is the number of protons, and,  $f_p$  ( $f_n$ ) is the DM-proton (-neutron) coupling. Due to isospin violation, the experiment's sensitivity is reduced, which implies that the restrictions on the cross section must be rescaled by the factor  $\sigma_p/\sigma_N^Z$ .

Taking into account both Eqs. (6) and (7), we find that the CRESST-III results do not impose constraints on the parameter space of the model. Thus, for the time being, this model can not be explored by DD experiments.

Since this model may not be currently probed through DD experiments, we consider other possibilities such as high-intensity proton beam experiments, e.g. DUNE [19] and SHiP [20]. These experiments have the capacity to explore sub-GeV DM models, and a discussion on this is found in Sec. IV. These experiment's sensitivity depends on  $\alpha_D$ ,  $\varepsilon$ , and the dark sector masses. For the aforementioned scenario ( $\alpha_D = 0.1$ ,  $m_{\gamma'} = 3m_{\phi_1}$ , and  $m_{\phi_2} = 1.0$  GeV), the relevant parameters for both the relic abundance and the sensitivity become then  $\varepsilon$  and  $m_{\gamma'}$ . Thus, we present the results of  $\Omega h^2$  (color map) in the plane of the two relevant parameters in Fig. 4. Since we want to compare to previous works such as [23], we also present the measured relic abundance for one component DM with the black dashed line and for the present model with the green dashed line. The plot shows that the two contours differ greatly, while the one component model is nearly diagonal, the two component has a triangular shape in the  $\varepsilon^2$ - $m_{\gamma'}$  plane. Here, we want to emphasize that even for the two component model, only one DM particle remains today, due to DM conversion. Nevertheless, the two DM particle model is very different to the one DM particle model, this in turn changes the portion of the parameter space where relic density is saturated.

#### IV. DARK MATTER AT HIGH-INTENSITY PROTON BEAM FACILITIES

High-intensity proton beam experiments provide a great opportunity to explore sub-GeV dark sectors. After the proton beam collision with the target, a large number of mesons are generated (such as  $\pi^0$  and  $\eta$ ) with a significant fraction of them decaying to two photons. A portion of those photons will convert into the dark photon thanks to the kinetic mixing. The dark photon then decays to two DM particles, and these particles will travel through Earth to the detector nearly unperturbed due to their weakly interacting nature. Once in the detector, they may interact with particles like electrons via the exchange of a photon-dark photon, see Fig. 5. Thus, to simulate the process, one must include the meson production and decay, DM production and interaction with the detector, as well as the neutrino background. This section describes the steps to simulate the aforementioned processes, in addition to the results on neutrino backgrounds.



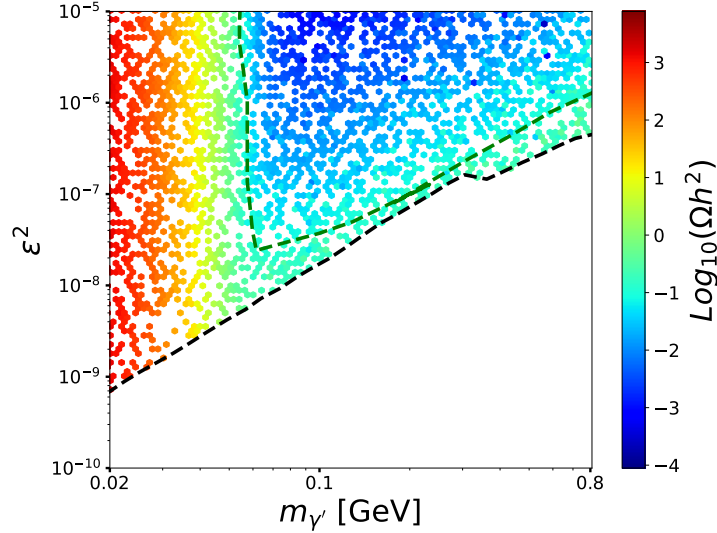


FIG. 4. Kinetic mixing vs. the dark photon mass where the color code denotes the relic density. The green (black) dashed line represents the points where the measured relic abundance is obtained for a two (one) DM component model.

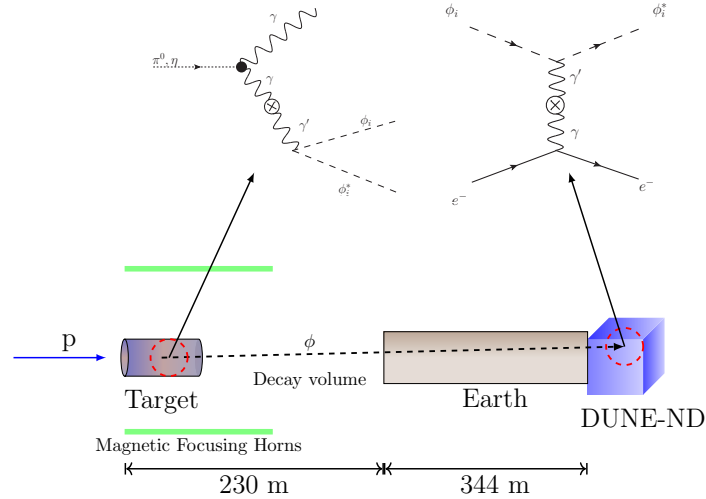


FIG. 5. Schematic illustration of DM searches at DUNE ND. A high intensity proton beam with an average energy of 120 GeV hits a fixed target made of carbon. After the collision, mesons are created and later decay to DM species which travel 574 m and interact with electrons in the DUNE ND.

### A. Fluxes

In high-intensity experiments, proton beams impact targets of diverse compositions (graphite and lead), resulting in the production of different particles. For instance, the collision produces neutral mesons (e.g.,  $\pi^0$  and  $\eta$ ) with rates depending on beam energy and target composition. In our case, the flux of these mesons was simulated with the help of the Monte Carlo generator PYTHIA 8.230 [41, 42]. In the case of relatively low-energy fixed target experiments, the flag `SoftQCD:all` is recommended to use [54]. Here, we consider the proton-carbon collision and hence the flux production of  $\pi^0$  and  $\eta$ ; studying the dominants decays of  $\pi^0 \rightarrow \gamma\gamma$  (BR  $\approx 98\%$ ),  $\eta \rightarrow \gamma\gamma$  (BR  $\approx 39\%$ ), and  $\eta \rightarrow 3\pi^0$  (BR  $\approx 33\%$ ) [55]. The table I displays the results obtained in the simulation of neutral-meson events normalized on the number of protons on target ( $N_{\text{POT}}$ ).

Neutral mesons decay just after their creation into photon pairs. These photons, via the kinetic mixing mechanism,

SoftQCD:a11		
Process	$pC \rightarrow \pi^0 \mathcal{X}$	$pC \rightarrow \eta \mathcal{X}$
N of part./ $N_{\text{POT}}$	4.1	0.50

TABLE I. Number of neutral mesons normalized to  $N_{\text{POT}}$  produced in the collision proton-Carbon ( $E_{\text{beam}} = 120$  GeV), simulated with PYTHIA and using the flag `SoftQCD:a11`. Here  $\mathcal{X}$  refers to other particles produced during the collision.

can give rise to the flux of dark photons via the process  $X \rightarrow \gamma\gamma'$  (being  $X = \pi^0$  or  $\eta$ ) and the subsequent decay of  $\gamma' \rightarrow \phi\phi^*$ <sup>1</sup>. This reaction can proceed via on-shell or off-shell  $\gamma'$ . Here, we consider the  $\gamma'$  decay is dominated by the on-shell mode. In that case, the branching ratio (under the narrow-width approximation) to the new channel fulfills [56, 57]

$$\text{Br}(X \rightarrow \gamma\phi\phi^*) \simeq \text{Br}(X \rightarrow \gamma\gamma) \times 2\varepsilon^2 \left(1 - \frac{m_{\gamma'}^2}{m_X^2}\right)^3 \text{Br}(\gamma' \rightarrow \phi\phi^*). \quad (8)$$

With  $X = \pi^0$  or  $\eta$ . Once produced, the DM candidates travel up to ND and interact with the electrons of the liquid argon via  $\phi e^- \rightarrow \phi^* e^-$  scattering.

Besides, charged mesons like pions and  $K$ -mesons, among others, are produced in the primary collision of the proton beam and target. In the case of DUNE, these charged mesons are collimated and selected by a system of magnetic horns. Depending on the orientation of the magnetic field of the horn, antimuons (muons) and two flavors of neutrino (antineutrino) survive after the decay of charged pions. Also,  $K^+(K^-)$ -mesons, among other particles, are selected by the horn. The muons and  $K$ -mesons decay to form the  $\nu_\mu, \nu_e$  or  $\bar{\nu}_\mu, \bar{\nu}_e$  fluxes. These fluxes are simulated by the collaboration DUNE, taking into account a series of effects, such as the interaction of the particles with the magnetic horn or the rock surrounding the beam [58]. The uncertainty in the simulation of the neutrino and antineutrino fluxes plays a crucial role in the physical program of LBNF, in particular, in oscillation physics [21]. After their production, the  $\nu_\mu, \nu_e$  or  $\bar{\nu}_\mu, \bar{\nu}_e$  fluxes travel to the ND, where they could interact with the electrons and nuclei of the liquid argon.

## B. Signal and Background at the DUNE Near Detector

It is relevant to find an approach, based on events distributions, to distinguish the recoil of electrons in DUNE ND produced by the DM candidates and neutrinos. The detector registers the recoil of electrons that ionize and scintillate the active material of the detector producing a signal that is recorded. Because of the forward-going nature of the electron track, neutrinos of the beam will produce events that look similar to DM signal through  $\nu e^- \rightarrow \nu e^-$  scattering ( $\nu - e$ ), which is purely electroweak process between neutrinos and atomic shell electrons<sup>2</sup>. Electrons can also appear via  $\nu_e$  induced Charged-Current Quasi-Elastic ( $\nu_e$ -CCQE) scattering or  $\nu_e {}^{40}\text{Ar} \rightarrow e^- \mathcal{N}$ , in which the final nucleon activity ( $\mathcal{N}$ ) is missed. Since the DUNE beam will operate in two horn currents, focusing positive and negative mesons producing a beam mostly composed of neutrinos and antineutrinos, respectively; each mode will drive out to different rates for the  $\nu_e$ -CCQE and  $\nu - e$  backgrounds.

To see the influence of these standard neutrino channels in the DM searches, we evaluate  $\nu - e$  and  $\nu_e$ -CCQE backgrounds using the NuWro event generator [43]. NuWro implements all important interactions in CC (charged currents) and NC (neutral currents) neutrino-nucleus processes and neutrino-electron scattering (channel added to the general module [44]). It is relevant to point out that although the  $\nu_e$  flux at DUNE ND is  $\sim 1\%$  of the total neutrino flux (in the on axis-position), the  $\nu_e$ -CCQE cross-section is over three orders of magnitude larger than the one for  $\nu - e$  scattering [21]. Nevertheless, the  $\nu_e$ -CCQE background can be reduced by choosing appropriate kinematical cuts; the electron recoil energy  $E_e$  and the electron angle with  $z$  axis  $\theta_e$ , particularly the composed function  $E_e\theta_e^2$ . The  $\nu - e$  scattering is constrained to  $E_e\theta_e^2 \leq 2m_e$  for a very forward electron along the direction of the neutrino beam (with  $E_e \ll E_\nu$  in the maximum value).

Since DM- $e$  scattering shares the same kinematical behavior of  $\nu - e$  with an identical topology in the Feynman diagrams, and hence the same cut  $E_e\theta_e^2 \leq 2m_e$ , the signal has a similar signature regarding  $\nu - e$  distribution. This fact converts  $\nu - e$  into an irreducible background according to signal spectrum in the  $E_e\theta_e^2$  quantity. The  $\nu_e$ -CCQE has

<sup>1</sup> We do not consider here the production of DM via proton bremsstrahlung  $pp \rightarrow pp\gamma'$  and the production process induced by leptonic secondary particles and their bremsstrahlung. In the kinematic region under consideration, these processes, if not negligible, are subdominant as it was shown in Ref. [24].

<sup>2</sup>  $\nu - e$  is not affected by hadrons or nuclear dynamics producing a clean signal of a very forward electron on the detector.



additional nuclear effects modifying the very forward nature for the outgoing electron, and therefore  $E_e\theta_e^2$  spectrum looks different to the signal, making it a reducible background [23]. DUNE ND will have the capability to reconstruct the electron energy with a resolution of 5% and the angle with a resolution of 12 mrad ( $E_e > 2$  GeV) [21]. With these values for DUNE ND, it is possible to compute the expected acceptance on  $E_e\theta_e^2$  giving a maximum of 2 MeV rad<sup>2</sup>. Using this resolution, it will be possible to cut more than 99% of events according to the electron energy and angle square in  $\nu_e$ -CCQE background (see appendix VIII A and table II for details). In what follows, we consider the impact of the  $\nu_e$ -CCQE-events distribution stored in  $E_e\theta_e^2 < 2$  MeV rad<sup>2</sup>.

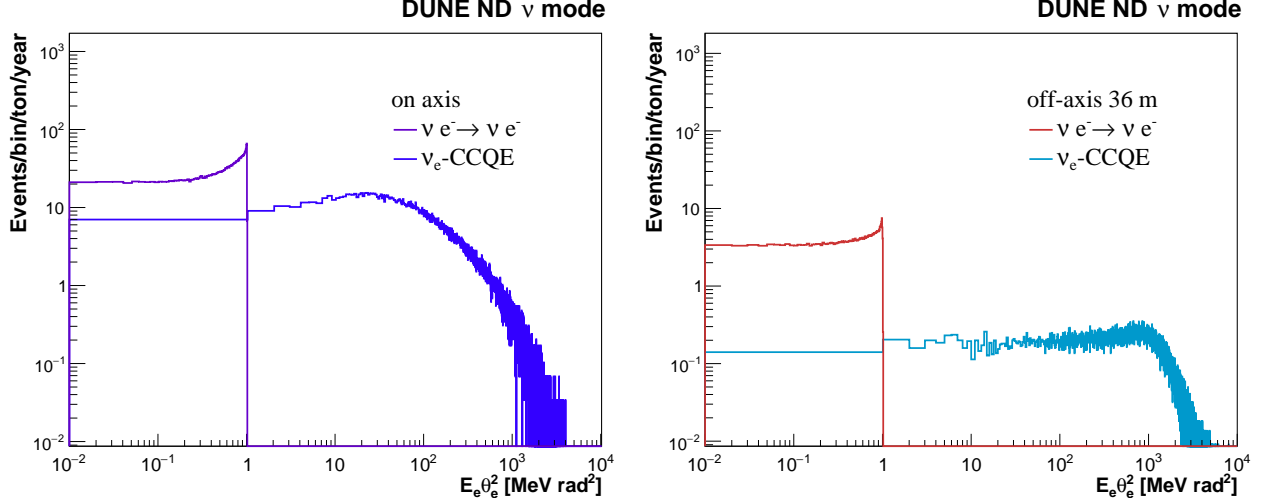


FIG. 6. Neutrino-electron and CCQE event rates as a function of the outgoing electron energy times angle squared for the extremal positions (on-axis and off-axis at 36 m) of the DUNE ND within  $\nu$  mode (normalized to total events/year/ton). Bin size for  $\nu_e$ -CCQE is 1 MeV rad<sup>2</sup> and for  $\nu - e$  is 0.01 MeV rad<sup>2</sup>.

Fig. 6 shows the  $E_e\theta_e^2$  distribution of  $\nu - e$  scattering and  $\nu_e$ -CCQE events in  $\nu$  mode for the on-axis and off-axis at 36 m. For both configurations of the detector, more than 99%  $\nu_e$ -CCQE background events have  $E_e\theta_e^2 > 2$  MeV rad<sup>2</sup>. This fact means that we can put a cut over this variable, which accepts the complete  $\nu - e$  background, and less than 0.5% the  $\nu_e$ -CCQE background.

In DUNE-PRISM, the presence of different neutrino flavors in different positions is a powerful tool to study signal-background sensitivity. Fig. 7 depicts the  $E_e\theta_e^2$  distribution of  $\nu - e$  scattering events for six off-axis positions in the  $\nu$  and  $\bar{\nu}$  modes without any cut of angular or energy resolution. The  $E_e\theta_e^2$  spectra show how  $\nu - e$  background decreases when the detector is moved across several off-axis positions. Besides, the normalized histograms for  $\nu - e$  events distribution are reduced when the beam is running in the anti-neutrino mode.

To find out critical discrepancies between signal and  $\nu - e$  background, we consider the spectrum of the final electron energy (bins of 0.25 GeV) in the on-axis and off-axis configurations. Fig. 8 displays  $\nu - e$  and DM - e signal for two benchmark scenarios in the maximal and minimal positions of the DUNE ND. For both on-axis and off-axis (36 m) positions of the LAr detector, the different background distribution profiles regarding the final electron energy provide an additional strength to search for DM at DUNE ND, since these discrepancies impact the signal-background ratio. The electron energy distribution works efficiently in the identification of reference points where signal and background differ, everything motivating a sensitivity study using this kinematic variable.

### C. The impact of constraints on sensitivity

In addition to the constraints coming from DM phenomenology given in section III A, we also took into account restrictions on the parameter space coming from B-factories and beam-dump experiments. The most stringent constraints of dark photon comes from BaBar searches. Light dark photon production at BaBar B factory, takes place via the reaction  $e^+e^- \rightarrow \gamma\gamma' \rightarrow \gamma + \text{invisible}$ , for  $m_{\gamma'} > 2m_{\text{DM}}$ , or  $e^+e^- \rightarrow \gamma\gamma' \rightarrow \gamma e^+e^-$ , when  $m_{\gamma'} < 2m_{\text{DM}}$  [59, 60]. The latter restriction corresponds to the gray region shown in Fig. 9. On the other hand, beam-dump experiments put limits on light DM produced via decay of neutral mesons which are produced in the collision of a proton ( or

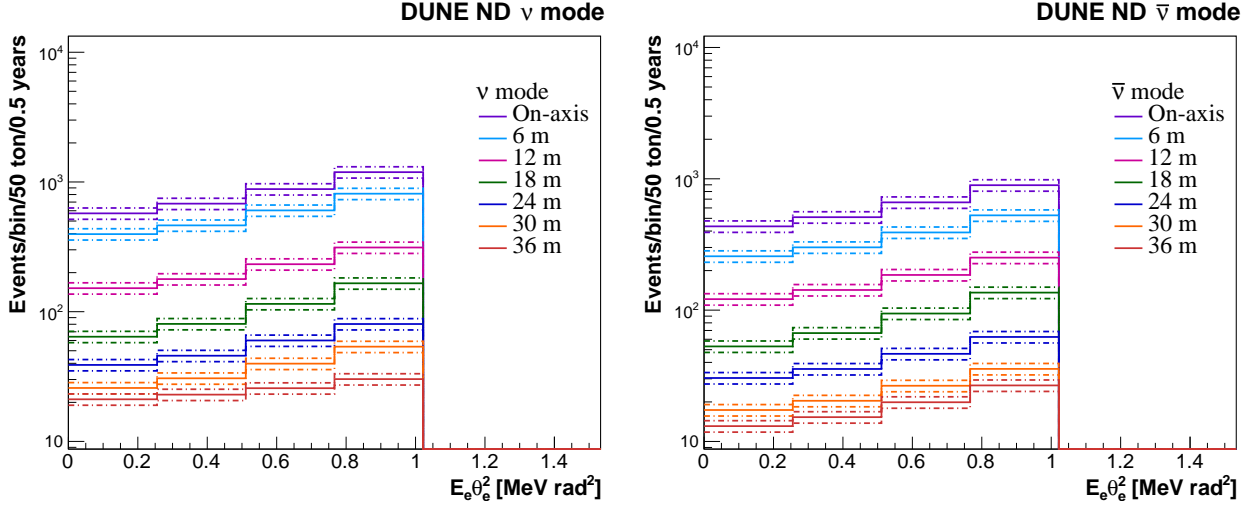


FIG. 7. Neutrino-electron event rates in the DUNE ND considering  $\nu$  (left) and  $\bar{\nu}$  (right) modes as a function of  $E_e \theta_e^2$  for the on-axis and six off-axis positions. Distributions allow a 10% normalization uncertainty for both of them (dashed-point line).

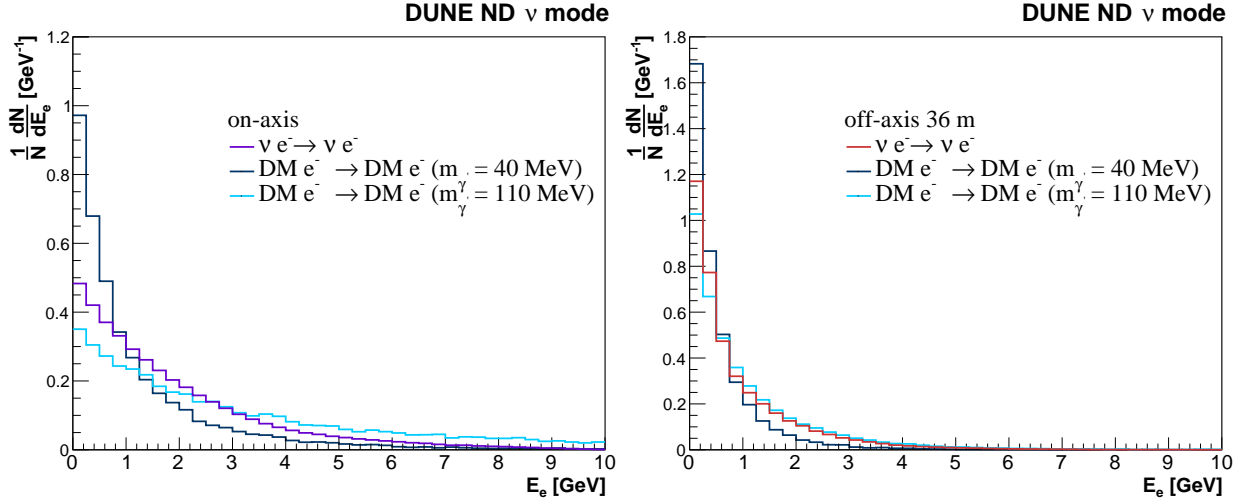


FIG. 8. Electron energy distribution for  $\nu - e$  background events (violet) and DM  $e^-$  scattering signal with  $m_{\gamma'} = 40$  MeV (dark blue) and  $m_{\gamma'} = 110$  MeV (cyan) for on-axis and one off-axis configuration at 36 m. In both positions, signals are constrained to have  $m_{\phi_1} = m_{\gamma'}/3$  and  $m_{\phi_2} = 1$  GeV.

electron) beam against a fixed target. The most stringent limit is imposed by NA64 [61, 62], which exclusion region is also displayed in the lighter gray in Fig. 9.

## V. SENSITIVITY ANALYSIS

The set of experiments used in the sensitivity analysis are briefly described in what follows.

- **DUNE:** In the case of DUNE ND, a proton beam at 120 GeV collides against a fixed target made of carbon. After the collision, a huge amount of particles are produced, among them, mesons, baryons, and other intermediate unstable particles. These particles later decay to photons, neutrinos, and other stable states. After that, the

photons, neutrinos, and neutral particles, including possible WIMPs travel 574 m until they reach the DUNE ND. The detector will have a fiducial mass of 50 tons of liquid argon and a rectangular parallelepiped shape with dimensions of 6 m wide, 2 m high and 3 m deep [63] (see schematic in Fig. 5). Inside the detector, the incoming neutrinos, as well as possible DM particles, scatter off electrons of the argon's atoms, leading to a signature with an energetic electron at the final state. The distinction between  $\nu - e$  scattering events (the background) and DM- $e$  scattering events (the signal) is achieved by comparing the electron recoil energy and  $E_e \theta_e^2$  distributions of both signatures. It is expected that over seven years of running, a total of  $7.7 \times 10^{21} N_{\text{POT}}$  will be delivered. The ND will be able to take data at different off-axis positions. Among other things, this will improve the potential exclusion reach of DUNE on the model because it increases the ratio between signal to background. On the other hand, the combination of all the results, those obtained for the on-axis and those for the off-axis configurations allows to explore a bigger parameter space in comparison with the use of the on-axis or off-axis data independently.

- **SHiP**: Regarding this experiment, a proton beam at 400 GeV hits a fixed target made of a thick heavy-metal hybrid [64]. In the collision, neutral stable particles are produced that then travel 38 m until reaching the Scattering Neutrino Detector (SND), where  $\nu - e$  scattering and DM- $e$  scattering take place. In five years of running a total of  $2 \times 10^{20} N_{\text{POT}}$  will be delivered.
- **NO $\nu$ A**: In this case a proton beam at 120 GeV strikes a 1.2 m graphite target. After the collision takes place, neutral stable particles (neutrino, DM species) are produced and then travel 990 m until reach NO $\nu$ A ND located 14.6 mrad away from the central axis of the neutrino beam. We used a  $2.97 \times 10^{20} N_{\text{POT}}$  of data taking [65–67] for the recasting analysis.

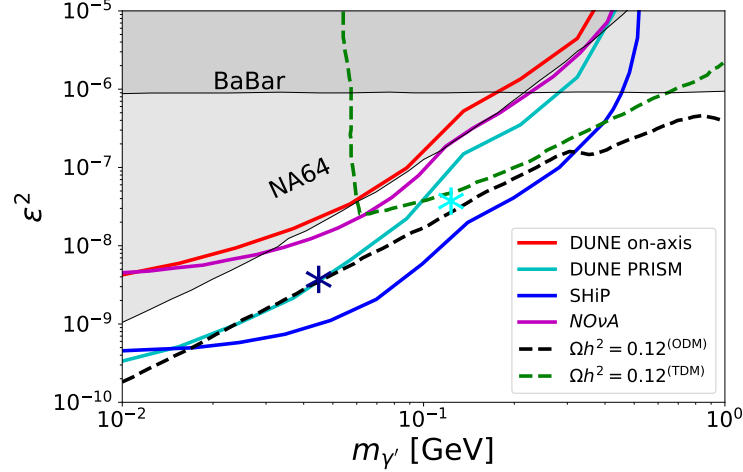


FIG. 9. Projected sensitivity at 90% CL. The red, cyan and blue solid line stand for the expected sensitivity of DUNE on-axis, DUNE-PRISM and SHiP respectively. The recasting of NO $\nu$ A is displayed in the magenta line and current constraints are given in the gray regions. The benchmark scenario considered in the analysis correspond to  $\alpha_D = 0.1$ ,  $m_{\gamma'} = 3m_{\phi_1}$  and  $m_{\phi_2} = 1.0$  GeV.

In Fig. 9, the results on the sensitivity and current exclusion limits are displayed as a function of the dark photon mass. The gray regions correspond to BABAR and NA64 experimental limits at 90% CL. The magenta line represents the current bound from NO $\nu$ A, the region above that line is excluded at 90% CL. The blue line stands for the potential reach on the sensitivity of SHiP experiment [64] assuming five years of running. The DUNE projection for the sensitivity are shown in the red and cyan lines for DUNE on-axis and DUNE PRISM configurations respectively.

Concerning the DUNE limits, the projected sensitivity for the on-axis and the DUNE PRISM configurations are both obtained using **MadDump** for signal simulation and **NuWro** for background simulation as described in Sec. II. In the analysis, it is assumed that the experiment will take data during seven years. *i*) For the DUNE on-axis analysis, 3.5 year in  $\nu$ -mode and 3.5 years in  $\bar{\nu}$ -mode and *ii*) for the DUNE PRISM analysis, we combine the results of on-axis position and different off-axis positions assuming that the detector takes data during 0.5 years in each mode ( $\nu$  and  $\bar{\nu}$ ) at different axis configurations, corresponding to vertical displacement of the detector from the beam axis of 0 m, 6 m, 12 m, 18 m, 24 m, 30 m and 36 m, respectively. We also used **MadDump** for signal simulations of SHiP and NO $\nu$ A.

Additionally, in Fig. 9 the dashed black and dashed green lines correspond to the thermal relic density equal to the experimental value observed by Planck satellite, for one dark matter candidate (ODM) and two dark matter candidates

(TDM), respectively. Finally, the cyan and dark blue stars represent the benchmark points displayed in Fig. 8. All in all, we conclude that by combining the on-axis with the off-axis data, the DUNE sensitivity increases around one order of magnitude in  $\epsilon^2$  for the explored mass range. Something that is interesting because it will, eventually, allow us to probe an unexplored region in the parameter space where the total relic density is in accordance with the observed one for ODM as well as for TDM candidates. Finally, the cyan and dark blue stars represent the benchmark points displayed in Fig. 8. Notice that these two benchmark points, so far, can only be probed by future DUNE PRIMS and SHiP experiments. We emphasize that for the TDM case, bounds coming from the thermal relic density and sensitivity allow us to explore a different region of the parameter space in comparison the ODM case. This result is novel and has not been reported in the literature. It is worth to mention that our sensitivity analysis results match those given in Refs. [23, 24]. For the sensitivity analysis we follow the statistical description given in appendix VIII B.

## VI. CONCLUSIONS

In this work, we have presented a DM model that includes two stable scalar singlets and a new broken  $U(1)_D$  symmetry. The model includes a massive dark photon that kinetically mixes with the SM photon. Thus, a DM candidate may communicate with SM particles through the photon-dark photon and with the other candidate through the dark photon portal. These two channels are very important in setting the relic abundance, but we find that DM conversion has a more profound effect because it dominates as long as it is viable. The result of this is that the heaviest DM particle converts into the lighter one, thus, only one DM particle remains. Nevertheless, the relic abundance phenomenology differs greatly from that of one DM particle. In fact, at the chosen benchmark point, for ODM the correct abundance has a diagonal shape in the  $\epsilon^2$ - $m_{\gamma'}$  plane, whereas the TDM has a triangular shape. This shape allows for different values of  $\epsilon^2$  at  $m_{\gamma'} \sim 0.06$  GeV, and shifts the allowed  $\epsilon^2$  for larger  $m_{\gamma'}$ . We also find that currently this model can not be probed through DD experiments such as CRESST-III.

Besides, we systematically study the relevant background for DM signals produced by neutrino interactions ( $\nu - e$ ) and  $\nu_e$ -CCQE at DUNE ND. We showed as less than 0.5% of  $\nu_e$ -CCQE events contribute to the total background for  $E_e \theta_e^2 < 2$  MeV rad<sup>2</sup>. We verify that the PRISM concept is critical in reducing the background events when the ND is moved for different off-axis positions. The possibility of cutting the  $\nu_e$ -CCQE background distributions and the advantages from the off-axis movement are crucial in the sensitivity studies.

Regarding the sensitivity analysis, we have found that projected sensitivity for DUNE on-axis for seven years of data taking will not have the potential to explore the model, mainly because the sensitivity limit at 90% CL will correspond to a region which is already excluded by NA64. The most important result comes from DUNE PRISM configuration that will improve the on-axis sensitivity by roughly one order of magnitude in  $\epsilon^2$ , thus, allowing this future configuration setup to test an unexplored region of the parameter space of the model. It turns out, that SHiP experiment, will be able to cover an even bigger fraction of the parameter space, because there are more control on the background. These experiments will open up a zone in the parameter space where the thermal relic density is fully explained for ODM as well as for TDM candidates, giving rise to the possibility to test the multiparticle nature of DM. The latter possibility, however, will depend on the ability of the experiment's detector to distinguishing signatures produced by different DM species at the detector. Additionally, as a complementary analysis, we recast the current limits provided by No $\nu$ A experiment, however, it does not put any additional restriction on the parameter space of the model, to the point that, the NA64 bound is slightly more stringent than No $\nu$ A.

## VII. ACKNOWLEDGMENTS

We are thankful to Liliana Sánchez, Óscar Zapata, Sandra Naranjo, Pedro Machado, Kevin Kelly, Yuber Perez, Dimitry Zhuridov, Luca Buonocore and the Maddump team for enlightening discussions. A.B, J.S and G.P are supported through Universidad EIA project grant II12019009. A.C is supported by the project grant 616-2019 from Minciencias-Universidad Sergio Arboleda (Postdoctoral National Programme). For the final stages of this work, A.C received a financial support of the “Flavor in the era of the LHC” project, grant PGC2018-102016-A-I00 funded by the Spanish MINECO.

## VIII. APPENDIX

### A. Total Expected Events for the Background

Distributions for  $\nu_e$ -CCQE and  $\nu - e$  backgrounds presented in Sec. IV B have considered the normalizations computed from exposure on DUNE ND, cross sections and neutrino fluxes. The number of events for the  $\nu_e$ -CCQE and  $\nu - e$  backgrounds are estimated via [68]

$$N_{\text{events}} = A_{\text{eff}} \bar{F} \times (\text{Target Particles}), \quad (9)$$

where  $\bar{F}$  is the relevant integrated neutrino flux. The effective area  $A_{\text{eff}}$  of the detector is

$$A_{\text{eff}} = \sigma \frac{M_D}{M_{\text{Ar}}} N_{\text{POT}}, \quad (10)$$

with  $\sigma$  the cross section per nucleon for  $\nu_e$ -CCQE or  $\nu - e$  scattering,  $M_D$  (units of atomic mass) the mass of the detector,  $M_{\text{Ar}}$  the mass of Argon (39.95 atomic mass), and  $N_{\text{POT}}$  is the number of protons on target per year.

To determine the overall events distribution, we analyze  $10^5$  CCQE  $\nu + {}^{40}\text{Ar}$  and  $\nu - e$  events generated in NuWro. To use the  ${}^{40}\text{Ar}$  spectral function, we set `nucleus.target=2` (Relativistic Fermi Gas) and `sf.method=1` (realistic density profile), and `cc_axial.mass=1030` MeV in the NuWro parameters-initialization file. When the target nucleon is bound in the parent nucleus, the Relativistic Fermi Gas Model (RFG) describes the initial nuclear state; the neutrons of Argon in the case of  $\nu_e$ -CCQE. Besides, the final state hadrons produced at the primary neutrino collision undergo non-perturbative effects of strong interactions inside the target nucleus. In this case, the absence of well-defined and complete models makes the treatment of these nuclear effects a relevant source of systematic uncertainty in the Montecarlo simulations [43, 69]. All other commands in the parameter card are the default values.

By using official neutrino fluxes at the near detector facility for the on-axis and on off-axis positions and running in the  $\nu$  - neutrino and antineutrino - modes [58] (design with a proton beam of 120 GeV) and the average cross-section given by NuWro, we compute the number of expected neutrino-electron scattering and  $\nu_e$ -CCQE events in the DUNE liquid argon near detector (listed in Tab II).

DUNE ND ( $\nu$ and $\bar{\nu}$ modes)							
Channel	On axis	6 m	12 m	18 m	24 m	30 m	36 m
$\nu_\mu e \rightarrow \nu_\mu e$	115	78	27	13	7	4	3
	12	10	5	3	2	1	1
$\nu_e e \rightarrow \nu_e e$	9	6	4	2	1	1	1
	3	2	2	1	0	0	0
$\bar{\nu}_\mu e \rightarrow \bar{\nu}_\mu e$	8	6	3	2	1	1	1
	82	45	20	9	5	3	2
$\bar{\nu}_e e \rightarrow \bar{\nu}_e e$	1	1	1	0	0	0	0
	3	2	1	1	0	0	0
<b>Total <math>\nu e \rightarrow \nu e</math></b>	133	91	35	17	9	6	5
	100	59	28	14	7	4	3
<b>Total <math>\nu_e</math>-CCQE</b>	3003	2355	1572	1067	750	550	412
	676	595	476	357	272	219	178
$\nu_e$ -CCQE*	14	10	6	3	2	1	0
	3	3	2	1	1	0	0

TABLE II. Expected number of  $\nu - e$  and  $\nu_e$ -CCQE events (per ton per year) in DUNE ND for on-axis and six off-axis positions. Events numbers in  $\nu$  ( $\bar{\nu}$ ) mode are in top (bottom) row. Fluxes consider  $0.125 < E_\nu < 10.125$  GeV. The last row for  $\nu_e$ -CCQE\* has the events accepted by the kinematical cut  $E_e \theta_e^2 < 2$  MeV rad<sup>2</sup>. The accepted events represent less than 0.5% of the total  $\nu_e$ -CCQE background.

## B. Statistical Analysis

In this section, we provide a description of the two different approaches used for building the statistical test applied in the analysis, ultimately both of them leading to equivalent results.

- **Log-likelihood:** Closely following the statistical test proposed in Refs [23, 25], we build a Poisson log-likelihood function to compare the signal plus background hypothesis against the background-only hypothesis<sup>3</sup>. For the signal as well as the background events, we consider the electron recoil energy distribution, with a total of 40 bins for energies in the range  $[0 - 10]$  GeV. The modified Poissonian likelihood function per energy bin  $j$  and detector position  $i$  reads

$$\mathcal{L}_{ij}(\mu) = \frac{(w_{ij})^{d_{ij}} e^{-(w_{ij})}}{d_{ij}!} \quad \text{with} \quad w_{ij} = Af_i(\mu N_{ij}^\phi + N_{ij}^\nu), \quad (11)$$

where  $N_{ij}^\nu$ ,  $N_{ij}^\phi$  and  $d_{ij}$  stands for number of background events, signal events, and observed events respectively, for each detector position  $i$  and energy bin  $j$ . The terms  $A$  and  $f_i$  are nuisance parameters for overall systematic uncertainty and detector positions respectively. Finally,  $\mu$  is a parameter which is set to 1 for signal plus background hypothesis and set to 0 for background-only hypothesis. Since for DUNE ND and SHiP there is not observed data, we assume  $d_{ij} = N_{ij}^\nu$  in the analysis. The binned test statistics is defined as

$$q = -2\Delta L = \sum_{i=1}^{n_{\text{pos}}} \left[ \sum_{j=1}^{n_{\text{bins}}} -2 \log \left( \frac{\mathcal{L}_{ij}(\mu=1)}{\mathcal{L}_{ij}(\mu=0)} \right) + \frac{(f_i - 1)^2}{\sigma_{f_i}^2} \right] + \frac{(A - 1)^2}{\sigma_A^2}, \quad (12)$$

where we assume  $\sigma_{f_i} = 1\%$  and  $\sigma_A = 10\%$ ,  $n_{\text{bins}}$  being the total number of bins and  $n_{\text{pos}}$  the total number of detector positions. A minimization of  $q$  respect to the nuisance parameters is performed in order to find them. By proceeding in such a way a total of  $n_{\text{pos}} + 1$  non-linear equations arises, allowing to obtain the nuisance parameters [70]. The sensitivity plots at 90% CL demands  $q > 4.61$  for two degrees of freedom.

- **Unbinned analysis:** The second possibility is to define the significance as [64, 71]:

$$Z = \frac{N^\phi}{\sqrt{N^\nu + \sum_{i \in (\nu_e, \nu_\mu, \bar{\nu}_e, \bar{\nu}_\mu)} (k_i N_i^\nu)^2}}, \quad (13)$$

where  $N^\phi$  corresponds to the total number of signal events,  $N^\nu$  the total background events,  $N_i^\nu$  the background events per each  $\nu$ -flavor background, and the  $k_i$  factors stand for the overall systematic uncertainty for each  $\nu$ -flavor background. For the sensitivity analysis,  $k_i = 10\%$  for DUNE and  $k_i = 5\%$  for SHiP are used, while for NO $\nu$ A, no uncertainties are considered. The sensitivity at 90% CL is obtained by setting  $Z \geq 1.64$ .

---

<sup>3</sup> For DUNE, events for signal and background are both simulated. In the case of NO $\nu$ A and SHiP, only signal events are simulated, the background are taking from the collaboration report [64–67].



- 
- [1] Brian Batell, Maxim Pospelov, and Adam Ritz, “Exploring Portals to a Hidden Sector Through Fixed Targets,” *Phys. Rev. D* **80**, 095024 (2009), [arXiv:0906.5614 \[hep-ph\]](#)
  - [2] Maxim Pospelov, Adam Ritz, and Mikhail B. Voloshin, “Secluded WIMP Dark Matter,” *Phys. Lett. B* **662**, 53–61 (2008), [arXiv:0711.4866 \[hep-ph\]](#)
  - [3] Maxim Pospelov, “Secluded U(1) below the weak scale,” *Phys. Rev. D* **80**, 095002 (2009), [arXiv:0811.1030 \[hep-ph\]](#)
  - [4] Marco Fabbrichesi, Emidio Gabrielli, and Gaia Lanfranchi, “The Dark Photon,” (5 2020), doi:“bibinfo doi 10.1007/978-3-030-62519-1, [arXiv:2005.01515 \[hep-ph\]](#)
  - [5] Hyun Min Lee and Min-Seok Seo, “Communication with SIMP dark mesons via Z’ -portal,” *Phys. Lett. B* **748**, 316–322 (2015), [arXiv:1504.00745 \[hep-ph\]](#)
  - [6] Daniel Feldman, Zuwei Liu, and Pran Nath, “The Stueckelberg Z-prime Extension with Kinetic Mixing and Milli-Charged Dark Matter From the Hidden Sector,” *Phys. Rev. D* **75**, 115001 (2007), [arXiv:hep-ph/0702123](#)
  - [7] Anson Hook, Eder Izaguirre, and Jay G. Wacker, “Model Independent Bounds on Kinetic Mixing,” *Adv. High Energy Phys.* **2011**, 859762 (2011), [arXiv:1006.0973 \[hep-ph\]](#)
  - [8] Mads T. Frandsen, Felix Kahlhoefer, Subir Sarkar, and Kai Schmidt-Hoberg, “Direct detection of dark matter in models with a light Z’,” *JHEP* **09**, 128 (2011), [arXiv:1107.2118 \[hep-ph\]](#)
  - [9] Giorgio Arcadi, Thomas Hugle, and Farinaldo S. Queiroz, “The Dark  $L_\mu - L_\tau$  Rises via Kinetic Mixing,” *Phys. Lett. B* **784**, 151–158 (2018), [arXiv:1803.05723 \[hep-ph\]](#)
  - [10] Eduardo Cortina Gil *et al.* (NA62), “Search for production of an invisible dark photon in  $\pi^0$  decays,” *JHEP* **05**, 182 (2019), [arXiv:1903.08767 \[hep-ex\]](#)
  - [11] Sabeeha Naaz, Jyotsna Singh, and R. B. Singh, “DUNE potential for sub-GeV dark matter in proton beam dump mode,” (12 2019), [arXiv:1912.08468 \[hep-ph\]](#)
  - [12] Juebin Lao, Chengfeng Cai, Zhao-Huan Yu, Yu-Pan Zeng, and Hong-Hao Zhang, “Fermionic and scalar dark matter with hidden U(1) gauge interaction and kinetic mixing,” *Phys. Rev. D* **101**, 095031 (2020), [arXiv:2003.02516 \[hep-ph\]](#)
  - [13] Eung Jin Chun, Jong-Chul Park, and Stefano Scopel, “Dark matter and a new gauge boson through kinetic mixing,” *JHEP* **02**, 100 (2011), [arXiv:1011.3300 \[hep-ph\]](#)
  - [14] K. S. Babu, Christopher F. Kolda, and John March-Russell, “Implications of generalized Z - Z-prime mixing,” *Phys. Rev. D* **57**, 6788–6792 (1998), [arXiv:hep-ph/9710441](#)
  - [15] B. Abi *et al.* (Muon g-2), “Measurement of the Positive Muon Anomalous Magnetic Moment to 0.46 ppm,” *Phys. Rev. Lett.* **126**, 141801 (2021), [arXiv:2104.03281 \[hep-ex\]](#)
  - [16] Gopolang Mohlabeng, “Revisiting the dark photon explanation of the muon anomalous magnetic moment,” *Phys. Rev. D* **99**, 115001 (2019), [arXiv:1902.05075 \[hep-ph\]](#)
  - [17] Alessandra Filippi and Marzio De Napoli, “Searching in the dark: the hunt for the dark photon,” *Rev. Phys.* **5**, 100042 (2020), [arXiv:2006.04640 \[hep-ph\]](#)
  - [18] Joel R. Primack, “Whatever happened to hot dark matter?,” *SLAC Beam Line* **31N3**, 50–57 (2001), [arXiv:astro-ph/0112336](#)
  - [19] Babak Abi *et al.* (DUNE), “Deep Underground Neutrino Experiment (DUNE), Far Detector Technical Design Report, Volume I Introduction to DUNE,” *JINST* **15**, T08008 (2020), [arXiv:2002.02967 \[physics.ins-det\]](#)
  - [20] Sergey Shirobokov (SHiP), “Search for New Physics with the SHiP experiment at CERN,” *PoS ICHEP2020*, 282 (2021)
  - [21] A. Abed Abud *et al.*, “Deep underground neutrino experiment (dune) near detector conceptual design report,” (2021), [arXiv:2103.13910 \[physics.ins-det\]](#)
  - [22] Chris M. Marshall, Kevin S. McFarland, and Callum Wilkinson, “Neutrino-electron elastic scattering for flux determination at the dune oscillation experiment,” *Physical Review D* **101** (Feb 2020), ISSN 2470-0029, doi:“bibinfo doi 10.1103/PhysRevD.101.032002, <http://dx.doi.org/10.1103/PhysRevD.101.032002>
  - [23] Valentina De Romeri, Kevin J. Kelly, and Pedro A. N. Machado, “DUNE-PRISM Sensitivity to Light Dark Matter,” *Phys. Rev. D* **100**, 095010 (2019), [arXiv:1903.10505 \[hep-ph\]](#)
  - [24] Andrea Celentano, Luc Darmé, Luca Marsicano, and Enrico Nardi, “New production channels for light dark matter in hadronic showers,” *Phys. Rev. D* **102**, 075026 (2020), [arXiv:2006.09419 \[hep-ph\]](#)
  - [25] Moritz Breitbach, Luca Buonocore, Claudia Frugiuele, Joachim Kopp, and Lukas Mitnacht, “Searching for Physics Beyond the Standard Model in an Off-Axis DUNE Near Detector,” (2 2021), [arXiv:2102.03383 \[hep-ph\]](#)
  - [26] Luca Buonocore, Claudia Frugiuele, and Patrick deNiverville, “Hunt for sub-GeV dark matter at neutrino facilities: A survey of past and present experiments,” *Phys. Rev. D* **102**, 035006 (2020), [arXiv:1912.09346 \[hep-ph\]](#)
  - [27] Marco Cirelli, Paolo Panci, Kalliopi Petraki, Filippo Sala, and Marco Taoso, “Dark Matter’s secret liaisons: phenomenology of a dark U(1) sector with bound states,” *JCAP* **05**, 036 (2017), [arXiv:1612.07295 \[hep-ph\]](#)
  - [28] Soo-Min Choi, Yonit Hochberg, Eric Kuflik, Hyun Min Lee, Yann Mambrini, Hitoshi Murayama, and Mathias Pierre, “Vector SIMP dark matter,” *JHEP* **10**, 162 (2017), [arXiv:1707.01434 \[hep-ph\]](#)
  - [29] Thomas Appelquist, Bogdan A. Dobrescu, and Adam R. Hopper, “Nonexotic Neutral Gauge Bosons,” *Phys. Rev. D* **68**, 035012 (2003), [arXiv:hep-ph/0212073](#)
  - [30] Babak Abi *et al.* (DUNE), “Deep Underground Neutrino Experiment (DUNE), Far Detector Technical Design Report, Volume II: DUNE Physics,” (2 2020), [arXiv:2002.03005 \[hep-ex\]](#)
  - [31] Adam Abed Abud *et al.* (DUNE), “Deep Underground Neutrino Experiment (DUNE) Near Detector Conceptual Design Report,” (3 2021), [arXiv:2103.13910 \[physics.ins-det\]](#)

- [32] John McDonald, “Gauge singlet scalars as cold dark matter,” *Phys. Rev. D* **50**, 3637–3649 (1994), [arXiv:hep-ph/0702143](#)
- [33] Vernon Barger, Paul Langacker, Mathew McCaskey, Michael Ramsey-Musolf, and Gabe Shaughnessy, “Complex Singlet Extension of the Standard Model,” *Phys. Rev. D* **79**, 015018 (2009), [arXiv:0811.0393 \[hep-ph\]](#)
- [34] Florian Staub, “SARAH 4 : A tool for (not only SUSY) model builders,” *Comput. Phys. Commun.* **185**, 1773–1790 (2014), [arXiv:1309.7223 \[hep-ph\]](#)
- [35] D. Aristizabal Sierra, Florian Staub, and Avelino Vicente, “Shedding light on the  $b \rightarrow s$  anomalies with a dark sector,” *Phys. Rev. D* **92**, 015001 (2015), [arXiv:1503.06077 \[hep-ph\]](#)
- [36] Werner Porod, “SPHeno, a program for calculating supersymmetric spectra, SUSY particle decays and SUSY particle production at  $e^+e^-$  colliders,” *Comput. Phys. Commun.* **153**, 275–315 (2003), [arXiv:hep-ph/0301101](#)
- [37] W. Porod and F. Staub, “SPHeno 3.1: Extensions including flavour, CP-phases and models beyond the MSSM,” *Comput. Phys. Commun.* **183**, 2458–2469 (2012), [arXiv:1104.1573 \[hep-ph\]](#)
- [38] Geneviève Bélanger, Fawzi Boudjema, Andreas Goudelis, Alexander Pukhov, and Bryan Zaldivar, “micrOMEGAs5.0 : Freeze-in,” *Comput. Phys. Commun.* **231**, 173–186 (2018), [arXiv:1801.03509 \[hep-ph\]](#)
- [39] J. Alwall, R. Frederix, S. Frixione, V. Hirschi, F. Maltoni, O. Mattelaer, H. S. Shao, T. Stelzer, P. Torrielli, and M. Zaro, “The automated computation of tree-level and next-to-leading order differential cross sections, and their matching to parton shower simulations,” *JHEP* **07**, 079 (2014), [arXiv:1405.0301 \[hep-ph\]](#)
- [40] Luca Buonocore, Claudia Fruguele, Fabio Maltoni, Olivier Mattelaer, and Francesco Tramontano, “Event generation for beam dump experiments,” *JHEP* **05**, 028 (2019), [arXiv:1812.06771 \[hep-ph\]](#)
- [41] Torbjörn Sjöstrand, Stefan Ask, Jesper R. Christiansen, Richard Corke, Nishita Desai, Philip Ilten, Stephen Mrenna, Stefan Prestel, Christine O. Rasmussen, and Peter Z. Skands, “An introduction to PYTHIA 8.2,” *Comput. Phys. Commun.* **191**, 159–177 (2015), [arXiv:1410.3012 \[hep-ph\]](#)
- [42] Torbjorn Sjostrand, Stephen Mrenna, and Peter Z. Skands, “PYTHIA 6.4 Physics and Manual,” *JHEP* **05**, 026 (2006), [arXiv:hep-ph/0603175](#)
- [43] T. Golan, J. T. Sobczyk, and J. Zmuda, “NuWro: the Wroclaw Monte Carlo Generator of Neutrino Interactions,” *Nucl. Phys. B Proc. Suppl.* **229-232**, 499–499 (2012)
- [44] Dmitry Zhuridov, Jan T. Sobczyk, Cezary Juszczak, and Kajetan Niewczas, “Monte carlo event generation of neutrino-electron scattering,” (2020), [arXiv:2007.14426 \[hep-ph\]](#)
- [45] N. Aghanim *et al.* (Planck), “Planck 2018 results. VI. Cosmological parameters,” *Astron. Astrophys.* **641**, A6 (2020), [arXiv:1807.06209 \[astro-ph.CO\]](#)
- [46] Eder Izaguirre, Gordan Krnjaic, Philip Schuster, and Natalia Toro, “Analyzing the Discovery Potential for Light Dark Matter,” *Phys. Rev. Lett.* **115**, 251301 (2015), [arXiv:1505.00011 \[hep-ph\]](#)
- [47] Patrick deNiverville and Claudia Fruguele, “Hunting sub-GeV dark matter with the NO $\nu$ A near detector,” *Phys. Rev. D* **99**, 051701 (2019), [arXiv:1807.06501 \[hep-ph\]](#)
- [48] Subhaditya Bhattacharya, Poullose Poullose, and Purusottam Ghosh, “Multipartite Interacting Scalar Dark Matter in the light of updated LUX data,” *JCAP* **04**, 043 (2017), [arXiv:1607.08461 \[hep-ph\]](#)
- [49] Ze-Peng Liu, Yue-Liang Wu, and Yu-Feng Zhou, “Enhancement of dark matter relic density from the late time dark matter conversions,” *Eur. Phys. J. C* **71**, 1749 (2011), [arXiv:1101.4148 \[hep-ph\]](#)
- [50] A. H. Abdelhameed *et al.* (CRESST), “First results from the CRESST-III low-mass dark matter program,” *Phys. Rev. D* **100**, 102002 (2019), [arXiv:1904.00498 \[astro-ph.CO\]](#)
- [51] Qing-Hong Cao, Ernest Ma, Jose Wudka, and C. P. Yuan, “Multipartite dark matter,” (11 2007), [arXiv:0711.3881 \[hep-ph\]](#)
- [52] Jonathan L. Feng, Jason Kumar, Danny Marfatia, and David Sanford, “Isospin-Violating Dark Matter,” *Phys. Lett. B* **703**, 124–127 (2011), [arXiv:1102.4331 \[hep-ph\]](#)
- [53] Carlos E. Yaguna, “Isospin-violating dark matter in the light of recent data,” *Phys. Rev. D* **95**, 055015 (2017), [arXiv:1610.08683 \[hep-ph\]](#)
- [54] Jeffrey M. Berryman, Andre de Gouvea, Patrick J Fox, Boris Jules Kayser, Kevin James Kelly, and Jennifer Lynne Raaf, “Searches for Decays of New Particles in the DUNE Multi-Purpose Near Detector,” *JHEP* **02**, 174 (2020), [arXiv:1912.07622 \[hep-ph\]](#)
- [55] P. A. Zyla *et al.* (Particle Data Group), “Review of Particle Physics,” *PTEP* **2020**, 083C01 (2020)
- [56] Patrick deNiverville, Maxim Pospelov, and Adam Ritz, “Observing a light dark matter beam with neutrino experiments,” *Phys. Rev. D* **84**, 075020 (2011), [arXiv:1107.4580 \[hep-ph\]](#)
- [57] S. Gardner, R. J. Holt, and A. S. Tadepalli, “New Prospects in Fixed Target Searches for Dark Forces with the SeaQuest Experiment at Fermilab,” *Phys. Rev. D* **93**, 115015 (2016), [arXiv:1509.00050 \[hep-ph\]](#)
- [58] Laura Fields, “Official dune fluxes,” <https://home.fnal.gov/~ljf26/DUNEFluxes/>
- [59] J. P. Lees *et al.* (BaBar), “Search for a Dark Photon in  $e^+e^-$  Collisions at BaBar,” *Phys. Rev. Lett.* **113**, 201801 (2014), [arXiv:1406.2980 \[hep-ex\]](#)
- [60] J. P. Lees *et al.* (BaBar), “Search for Invisible Decays of a Dark Photon Produced in  $e^+e^-$  Collisions at BaBar,” *Phys. Rev. Lett.* **119**, 131804 (2017), [arXiv:1702.03327 \[hep-ex\]](#)
- [61] Dipanwita Banerjee (NA64, Physics Beyond Colliders Conventional Beams Working Group), “Search for Dark Sector Physics at the NA64 experiment in the context of the Physics Beyond Colliders Projects,” *PoS LeptonPhoton2019*, 061 (2019), [arXiv:1909.04363 \[hep-ex\]](#)
- [62] Yu. M. Andreiev *et al.* (NA64), “Constraints on New Physics in Electron  $g - 2$  from a Search for Invisible Decays of a Scalar, Pseudoscalar, Vector, and Axial Vector,” *Phys. Rev. Lett.* **126**, 211802 (2021), [arXiv:2102.01885 \[hep-ex\]](#)
- [63] Adam Abed Abud *et al.* (DUNE), “Deep Underground Neutrino Experiment (DUNE) Near Detector Conceptual Design Report,” (3 2021), [arXiv:2103.13910 \[physics.ins-det\]](#)

- [64] C. Ahdida *et al.* (SHiP), “Sensitivity of the SHiP experiment to light dark matter,” *JHEP* **04**, 199 (2021), [arXiv:2010.11057 \[hep-ex\]](#)
- [65] Jianming Bian, “Measurement of Neutrino-Electron Elastic Scattering at NOvA Near Detector,” in *Meeting of the APS Division of Particles and Fields* (2017) [arXiv:1710.03428 \[hep-ex\]](#)
- [66] M. A. Acero *et al.* (NOvA), “Measurement of neutrino-induced neutral-current coherent  $\pi^0$  production in the NOvA near detector,” *Phys. Rev. D* **102**, 012004 (2020), [arXiv:1902.00558 \[hep-ex\]](#)
- [67] M. A. Acero *et al.* (NOvA), “First Measurement of Neutrino Oscillation Parameters using Neutrinos and Antineutrinos by NOvA,” *Phys. Rev. Lett.* **123**, 151803 (2019), [arXiv:1906.04907 \[hep-ex\]](#)
- [68] Carsten Rott, Seongjin In, Jason Kumar, and David Yaylali, “Directional searches at dune for sub-gev monoenergetic neutrinos arising from dark matter annihilation in the sun,” *Journal of Cosmology and Astroparticle Physics* **2017**, 016–016 (Jan 2017), ISSN 1475-7516, <http://dx.doi.org/10.1088/1475-7516/2017/01/016>
- [69] L. Alvarez-Ruso, M. Sajjad Athar, M.B. Barbaro, D. Cherdack, M.E. Christy, P. Coloma, T.W. Donnelly, S. Dytman, A. de Gouvêa, R.J. Hill, and et al., “Nustec white paper: Status and challenges of neutrino–nucleus scattering,” *Progress in Particle and Nuclear Physics* **100**, 1–68 (May 2018), ISSN 0146-6410, <http://dx.doi.org/10.1016/j.pnpnp.2018.01.006>
- [70] J. S. Conway, “Incorporating Nuisance Parameters in Likelihoods for Multisource Spectra,” in *PHYSTAT 2011* (2011) [arXiv:1103.0354 \[physics.data-an\]](#)
- [71] P. A. Zyla *et al.* (Particle Data Group), “Review of Particle Physics,” *PTEP* **2020**, 083C01 (2020)